ACS APPLIED MATERIALS & INTERFACES

Research Article

www.acsami.org

Chlorin e6-Encapsulated Polyphosphoester Based Nanocarriers with Viscous Flow Core for Effective Treatment of Pancreatic Cancer

Fei Ding,[†,§] Hong-Jun Li,[‡,§] Jun-Xia Wang,[⊥,§] Wei Tao,[⊥] Yan-Hua Zhu,[⊥] Yue Yu,[*,†] and Xian-Zhu Yang[*,⊥]

[†]Division of Gastroenterology, Affiliated Provincial Hospital, Anhui Medical University, No.17 Lu Jiang Road, Hefei, Anhui 230001, China

[‡]The CAS Key Laboratory of Innate Immunity and Chronic Disease, School of Life Sciences and Medical Center, University of Science & Technology of China, Hefei, Anhui 230027, P.R. China

[⊥]Department of Medical Materials and Rehabilitation Engineering, School of Medical Engineering, Hefei University of Technology, Hefei, Anhui 230009, China

Supporting Information

ABSTRACT: Lack of effective treatment results in the low survival for patients with pancreatic cancer, and photodynamic therapy (PDT) with photosensitizers has emerged as an effective therapeutic option for treatment of various tumors by light-generated cytotoxic reactive oxygen species (ROS) to induce cell apoptosis or necrosis. However, the poor solubility, rapid blood clearance, and weak internalization of the photosensitizer seriously inhibit its anticancer efficacy. To overcome these obstacles, a polyphosphoester-based nanocarrier (NP-PPE) is employed as the carrier of the hydrophobic photosensitizer, chlorin e6 (Ce6), for photodynamic therapy. The Ce6-encapsulated nanocarrier (NP-PPE/Ce6) significantly promoted the cellular internalization of Ce6, enhanced the generation of ROS in the tumor cells after irradiation. Therefore, the cellular phototoxicity of NP-PPE/Ce6 against BxPC-3 pancreatic cancer cells was markedly enhanced than that of free Ce6 in vitro. Furthermore, NP-PPE/Ce6 improved accumulation of Ce6 in tumor tissue and treatment with NP-PPE/Ce6 significantly enhanced antitumor efficacy in human BxPC-3 pancreatic cancer xenografts. These results suggest that using a polyphosphoester-based nanocarrier as the delivery system for a photosensitizer has great potential for PDT of pancreatic cancer.

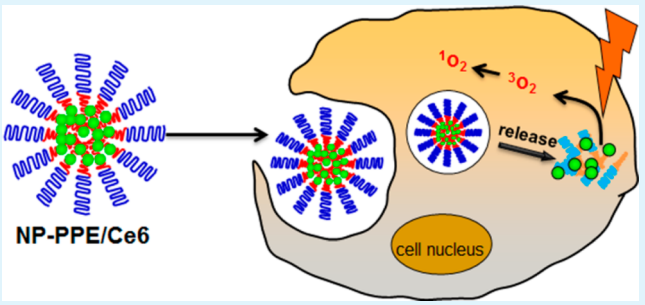

KEYWORDS: *photodynamic therapy, polyphosphoester, nanomedicine, drug delivery, pancreatic cancer*

INTRODUCTION

Pancreatic cancer is an aggressive and devastating disease, which is characterized by invasiveness, rapid progression, and profound resistance to treatment.[1] The median survival of metastatic pancreatic was only about six months, and related survey revealed the overall five year survival rate was less than 5%.[2] As the unique approved treatment agent for pancreatic cancer in clinical trials, unfortunately, gemcitabine showed poor efficacy, drug resistance, and side effects.[3−5] It is desired to develop effective methods to improve the therapeutic efficacy in clinical trials.

Photodynamic therapy (PDT) has emerged as an efficient medical tool for treating various cancers.[6−9] When the proper wavelength of light irradiates photosensitizers, highly reactive ROS are generated.[10] The ROS was able to destroy tumor by multifactorial mechanisms, including directly inducing tumor cell death by necrosis or apoptosis, destruction of tumor vasculatures as an antiangiogenesis effect, and also the stimulation of the host immune system to recognize.[9,11−15] In addition, the photosensitizers itself is minimally toxic in the absence of light irradiation, thus the accumulation of photosensitizers in other organs show minimally systemic toxic. In addition, the activating light, which is nonionizing, is no harmful for tissues without photosensitizers compare with radiotherapy.[16] In recent years, PDT has emerged as an increasingly recognized alternative to classical cancer therapies such as radiotherapy and chemotherapy.[17] However, poor water solubility of photosensitizers limited broad clinical applications of PDT, resulting in rapid clearance in blood circulation, inefficient accumulation, and internalization.

To overcome the predicament, a variety of nanocarriers were developed as the delivery systems of photosensitizers in the past few years, such as inorganic nanoparticles, liposome, polymeric nanoparticle, and so on.[18−23] These nanocarriers can increase photosensitizers' solubility either by physical encapsulation or by chemical conjugation, as well as prolong the blood

Received: June 26, 2015
Accepted: August 12, 2015
Published: August 12, 2015

DOI: 10.1021/acsami.5b05724
ACS Appl. Mater. Interfaces 2015, 7, 18856−18865

circulation time and enhance the accumulation of photosensitizers in tumor tissue via the enhanced permeability and retention (EPR) effect. Among these nanocarriers, liposomes have been widely used due to their suitability for packaging large quantities of hydrophobic photosensitizers. Additionally, polymeric nanoparticles are also attractive since the highly maneuverable and satisfying biocompatibility.[23] However, the photosensitizers which encapsulated or conjugated in the hydrophobic core of the polymeric nanoparticle usually composed of polylactic acid (PLA), poly(lactic-*co*-glycolic) acid (PLGA) or poly(ε-caprolactone) (PCL) result in a conspicuous reduction of singlet oxygen by self-quenching which could reduce PDT efficiency.[24−27] Therefore, it is urgently desired to design polymeric nanocarriers, which can rapidly release the photosensitizers after internalization for promoted PDT efficiency in cancer therapy.

Recently, we have found that the encapsulated cargo release from hydrophobic polyphosphoester based polymeric nanocarrier is significantly faster than that from PLA based nanoparticles, because hydrophobic polyphosphoesters were in a viscous flow state at room temperature.[28] Herein, we developed photosensitizers loaded polyphosphoester based nanocarriers for near-infrared light (NIR) photodynamic therapy (Scheme 1).

Scheme 1. Schematic Illustration of (A) the Process Preparing NP-PPE/Ce6 by Self-Assembly of Amphiphilic mPEG-*b*-PHEP Copolymer and Ce6, (B) the Nanocarrier Promoting Cellular Internalization of Ce6 and Releasing Them Intracellularily[a]

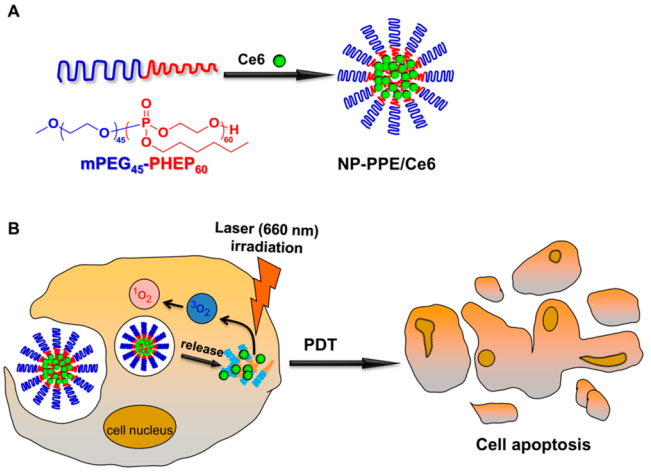

[a]The photosensitizer Ce6 can generate reactive oxygen species (ROS) with NIR laser irradiation to kill the cancer cells.

Chlorin e6 (Ce6) was selected as the photosensitizers since its high sensitizing efficacy and high fluorescent emission at long wavelengths of 660−670 nm, which can offer a clear window and ideal penetration for optical image and PDT in vivo.[29−32] Their physiochemical characters, including size, shape, stability, and release rate were systematically evaluated. In vitro endocytosis, subcellular localization, and the generation of cytotoxic ROS plus irradiation were comprehensively evaluated. The cytotoxic effects of polyphosphoester based nanocarriers were also investigated and compared in BxPC-3 pancreatic cancer cells. Moreover, the pharmacokinetics, biodistribution, and overall antitumor efficacy to BxPC-3 xenograft tumors were evaluated in vivo.

EXPERIMENTAL SECTION

Materials. Photosensitizer chlorin e6 (Ce6) was purchased from J&K Chemical Ltd. (Shanghai, China). Methyl thiazol tetrazolium (MTT), $mPEG_{45}$-OH and 1,5,7-triazabicylo[4.4.0]dec-5-ene (TBD) were purchased from Sigma-Aldrich. Featal bovine serum (FBS), 4,6-diamidino-2-phenylindole (DAPI), Alexa Fluor 488 phalloidin, and dichlorofluorescein diacetate (DCFH-DA) were obtained from Invitrogen (Carlsbad, NM). Trypsin-EDTA was purchased from Gibco BRL (Eggenstein, Germany). Other solvents and chemicals were of analytical level and used as received. Pancreatic cancer cells BxPC-3 were from the American Type Culture Collection (ATCC).

The amphiphilic diblock copolymer mPEG-*b*-PHEP was synthesized using $mPEG_{45}$-OH as the macroinitiator under the catalysis of TBD as described in the Supporting Information. The critical micelle concentration (CMC) of the obtained amphiphilic copolymers mPEG-*b*-PHEP was detected using the fluorescence probe pyrene as previously described.[28]

Preparation and Characterization of Ce6-Loaded Polyphosphoester Based Nanocarriers (NP-PPE/Ce6). First, photosensitizer Ce6 (10.0 mg/mL in DMSO, 0.1 mL) and polymer $mPEG_{45}$-*b*-$PHEP_{60}$ (10.0 mg/mL in DMSO, 1.0 mL) were mixed and stirred for 20 min. Then the water (20.0 mL) was added dropwise and continually stirred for another 4 h at room temperature. Finally, the solution was transferred to dialysis tube (cutoff molecular weight was 3500) and dialyzed against ultrapure water for 2 days. In addition, the final solution was filtered through a 0.45 μm filter (Millipore) to remove unloaded Ce6 and the obtained Ce6-loaded nanocarriers (NP-PPE/Ce6). To test the Ce6 loading efficiencies, the drug-loaded nanocarriers were lyophilized and weighed, and the product was redissolved with DMSO. The concentration of Ce6 was determined using a UV−vis spectrometer (UV-2802 PC, UNICO Instruments) at 405 nm wavelengths and referring to a standard curve of free Ce6 concentrations in DMSO. The loading content (DLC) and loading efficiencies (LE) were calculated by the following equations:

$$\text{DLC}\ (\%) = \frac{\text{amount of Ce6 in nanocarrier}}{\text{amount of Ce6-loaded nanocarrier}} \times 100\%$$

$$\text{LE}\ (\%) = \frac{\text{amount of Ce6 in nanocarrier}}{\text{amount of Ce6 added}} \times 100\%$$

The size distribution, polydispersion index (PDI), and zeta potential of the nanocarriers was determined by dynamic light scattering (DLS) (Malvern ZS 90, England). Morphology of nanoparticle was examined by JEOL-2010 transmission electron microscopy (TEM, JEOL Co., Ltd., Tokyo, Japan) at an accelerating voltage of 200 kV.

Monitoring the Stability of NP-PPE/Ce6 and Ce6 Releasing from NP-PPE/Ce6. To monitor the stability of NP-PPE/Ce6 in the mimic physiological conditions, NP-PPE/Ce6 was incubated in phosphate buffered saline (PBS, pH 7.4, 0.01 M) containing with 10% FBS at 37 °C with gentle stirring. At each predetermined point time, the diameter of NP-PPE/Ce6 was measured with DLS.

To monitor the release profile of Ce6 in the mimic extracellular and intracellular condition, NP-PPE/Ce6 solution was packed in dialysis tube (cutoff molecular weight was 14,000). Then the tubes were dipped in 20 mL phosphate buffer (0.02 M, pH value was 5.5 and 7.4) with 0.1% Tween-80. During the studies, the solution of the each buffer was gently shaken at 100 rpm at 37 °C. The external PB solution was continuously collected at predetermined times, freeze-dried, and redissolved in methanol and the concentration of Ce6 was determined by high-performance liquid chromatography (HPLC) analyses, using a Waters HPLC system consisting of a Waters 1525 binary pump, a Waters 2487 UV/visible detector, a 1500 column heater, and a Symmetry C18 column. The UV/visible detector was set at 405 nm and linked to Breeze software for data analysis. HPLC grade ammonium acetate buffer (0.05 M, pH 5.5) with methanol at a ratio of 38:62 (v/v) was used as the mobile phase at 30 °C with a flow rate of 0.7 mL min^{-1}. Linear calibration curves for concentrations in the range of 1.0−32.0 μg/mL were constructed using the peak areas by linear

DOI: 10.1021/acsami.5b05724
ACS Appl. Mater. Interfaces 2015, 7, 18856−18865

regression analysis. The concentration of Ce6 in the solution was calculated based the standard curve.

Detect the Fluorescence Quenching and ROS Generation of NP-PPE/Ce6. To detect the fluorescence quenching and recovery of NP-PPE/Ce6 in different conditions, the NP-PPE/Ce6 was incubated in different conditions (PB buffer, 0.02 M, pH 7.4 or 5.5) at 37 °C. After predetermined time incubation, the fluorescence intensity of the solutions was detected by Shimadzu RF-5301PC spectrofluorophotometer.

The ability of ROS generation of NP-PPE/Ce6 in different conditions was determined by spectrofluorophotometer using dichlorofluorescein diacetate (DCFH-DA) as an indicator. First, reactivity of the DCFH solution was resulted from the chemical hydrolysis of DCFH-DA at basic pH. Then solution of Ce6, original NP-PPE/Ce6 and NP-PPE/Ce6 pretreatment in the pH 5.5 PB buffer for 12 h was added into the solution of DCFH. Then these solutions were exposed to the NIR laser (660 nm, 0.5 mW/cm^2) for 30 min, then the ROS concentration was determined through measuring the fluorescence intensity of DCF (Ex = 488 nm, Em = 525 nm).

In Vitro Cellular Uptake of NP-PPE/Ce6. Pancreatic cancer cells BxPC-3 were cultured with RPMI 1640 containing 10% fetal bovine serum. To measure the cellular uptake of NP-PPE/Ce6, cells were seeded in 24-well plates (1.0×10^6 cells/well) and incubated at 37 °C for 24 h. Then the medium was replaced with 0.5 mL of serum-free medium which contained NP-PPE/Ce6 or Ce6 respectively (2.5 μg/mL of Ce6). After further incubation for 2 or 4 h, the cells were washed three times with PBS, trypsinized and collected for FACS analyses (FACS Calibur flow cytometer, BD Biosciences, USA).

For quantitatively detecting the cellular uptake of Ce6, BxPC-3 cells were seeded in 12-well plates (1.0×10^6 cells/well). After incubation for 24 h, the medium was replaced with 1.0 mL serum-free medium containing NP-PPE/Ce6 or free Ce6 at an equivalent Ce6 concentration of 10.0 μg/mL. Further incubation for 2 or 4 h, the cells were washed with PBS and then trypsinized. Finally, the concentration of Ce6 in the cancer cells was determined by HPLC.

Additionally, the cellular uptake of NP-PPE/Ce6 or free Ce6 was determined by confocal laser scanning microscope (CLSM, LSM 710, Carl Zeiss Inc., Germany), the BxPC-3 cells were seeded on coverslips in 12-well plates and incubated for 24 h. The medium was replaced with 1.0 mL serum-free medium containing free Ce6 or NP-PPE/Ce6, respectively (20 μg/mL of Ce6). After further incubation for 2 or 4 h, the cells were washed with PBS, fixed with 4% paraformaldehyde for 15 min at room temperature. The cytoskeleton and nucleus were stained with Alexa Fluor 488 phalloidin and DAPI according to the standard protocol provided by the suppliers. The cellular uptake of Ce6 was visualized by CLSM.

Phototoxicity Assays of NP-PPE/Ce6 in Vitro. BxPC-3 cells were seeded onto 96-well plates (5.0×10^3 cells/well) and incubated for 24 h. Then the medium was replaced with 100 μL of medium containing free Ce6 or NP-PPE/Ce6 at different concentrations. After incubation for 12 h, the partial groups were irradiated with near-infrared laser (660 nm, 0.5 W/cm^2) for 20 min. Finally, all the groups were incubated at 37 °C for 1 day. MTT assay was used to measure the cell viability according to the standard protocol.

For monitoring the cell apoptosis, BxPC-3 cells were seeded onto 12-well cell culture plates (1.0×10^6 cells/well) overnight. After that, the medium was replaced with 1 mL medium containing NP-PPE/Ce6 or free Ce6 (0.5 μg/mL of Ce6) for 12 h. Then, partial group were exposed to NIR laser (660 nm, 0.2 W/cm^2) for 20 min. After further incubation for 24 h, cells were washed with PBS for 3 times and stained with trypan blue solution (0.4% in PBS) for 5 min. Microscopic images of cells were then taken using a Nikon TE2000 microscope.

Generation of ROS from NP-PPE/Ce6 in the Cell. To detect the generation of ROS from NP-PPE/Ce6, BxPC-3 cells were seeded in 24-well plates (1.0×10^6 cells/well) at 37 °C. After incubation for 24 h, the medium was replaced with 0.5 mL serum-free medium which contained NP-PPE/Ce6 (15 μg/mL of Ce6) or free Ce6 (15 μg/mL) and incubated for 12 h. Then the active oxygen detection reagent DCFH-DA (10 μmol/mL) was added and incubated for 30 min. Then cells were irradiated with NIR laser (660 nm, 0.5 W/cm^2) for 30 min. Finally, the green fluorescent signal of DCF, which indicated the generation of singlet oxygen in the cells, was detected using fluorescence microscope (Ex = 488 nm, Em = 525 nm).

Pharmacokinetics, Biodistribution, and Accumulation of NP-PPE/Ce6 in Vivo. Balb/C nude mice (4−5 weeks) and ICR mice (5−6 weeks) were prepared by the Beijing HFK Bioscience Co., Ltd. All animals received care in compliance with the guidelines outlined in the Guide for the Care and Use of Laboratory Animals. The procedures were approved by the University of Science and Technology of China Animal Care and Use Committee.

To detect the blood clear features of NP-PPE/Ce6 or free Ce6, ICR mice were randomly divided into two groups. NP-PPE/Ce6 and free Ce6 were intravenously injected into ICR mice through the tail vein at a dose of 2.5 mg/kg (n = 3 per group). And then the blood samples collected at different time points after injection (5 and 30 min, 1, 2, 4, 8, 12, 24, and 48 h). The blood samples were placed in 1.5 mL EP tubes coated with heparin sodium. Finally, the blood samples were treated and the concentration of Ce6 in the plasma of each group was measured by HPLC. The pharmacokinetics parameters were calculated were calculated by DAS 3.0 with the noncompartmental model.

In order to monitor biodistribution of free Ce6 and NP-PPE/Ce6 in vivo, Balb/C nude mice (4−5 weeks) were used to establish a human pancreatic xenograft tumor model by subcutaneous injection of BxPC-3 cells (10^7 cells/mouse) into the right side of the back. When the tumor volume reached about 200−300 mm^3, 500 μL of PBS, NP-PPE/Ce6 or free Ce6 (containing 350 μg of Ce6) were injected into the tail vein. At the predetermined times, the mice were anaesthetized and imaged with a Xenogen IVIS Lumina system (Caliper Life Sciences, USA). In addition, the mice were sacrificed, and the tumor tissues and organs were collected and imaged by a Xenogen IVIS Lumina system. Then, the organs were weighted and homogenized, and the Ce6 distribution was determined after extraction by HPLC as mentioned above.

Photodynamic Therapeutic Efficacy of NP-PPE/Ce6 in BxPC-3 Tumor-Bearing Mice. To evaluate the photodynamic therapeutic efficacy in vivo, tumor models were established as described above. When the tumor size reached nearly 125 mm^3, PBS, NP-PPE/Ce6, or free Ce6 with an equivalent Ce6 dose of 2.5 mg/kg were intravenously injected through the tail vein (n = 5 per group). At 4 h postinjection, the mice of NP-PPE/Ce6 group (w Laser) and Ce6 group (w Laser) were exposed to near-infrared light (660 nm, 0.5 W/cm^2) for 30 min at the tumor site. The mice without irradiation were used as the control. The photodynamic therapeutic efficacy was evaluated by measuring the tumor volumes, which was calculated according to the following formula: tumor volume (mm^3) = 0.5 × length × width^2. After 16 days postinjection, the mice were killed, and the tumors tissues were excised to measure the wet weight. Then, tumor tissues and main organs were fixed in 4% formaldehyde and embedded in paraffin. Then, the slices were prepared and stained with hematoxylin and eosin (H&E). In addition, the tumor sections were acquired for immunnohistochemical staining of the terminal transferase dUTP nick-end labeling (TUNEL) assay and the proliferating cell nuclear antigen (PCNA).

Statistical Analysis. Quantitative data were expressed as mean standard deviations unless specifically described. Means were compared using student's t test. P values <0.05 were considered statistically significant.

RESULTS AND DISCUSSION

Physicochemical Characteristics of Ce6 Encapsulated Nanoparticle. The amphiphilic diblock copolymers mPEG-b-PHEP was synthesized using mPEG$_{45}$-OH as the macroinitiator and TBD as the catalyst. The obtained polymers were analyzed by GPC and NMR. As shown in Figure 1A, the obtained polymers exhibited unimodal peaks toward higher molecular weights compared with the mPEG$_{45}$-OH macroinitiator. The polydispersity of the obtained diblock copolymer mPEG-b-PHEP was 1.23, estimated by GPC measurement using polystyrene standards. In addition, the ^{1}H NMR spectra (Figure 1B)

DOI: 10.1021/acsami.5b05724
ACS Appl. Mater. Interfaces 2015, 7, 18856−18865

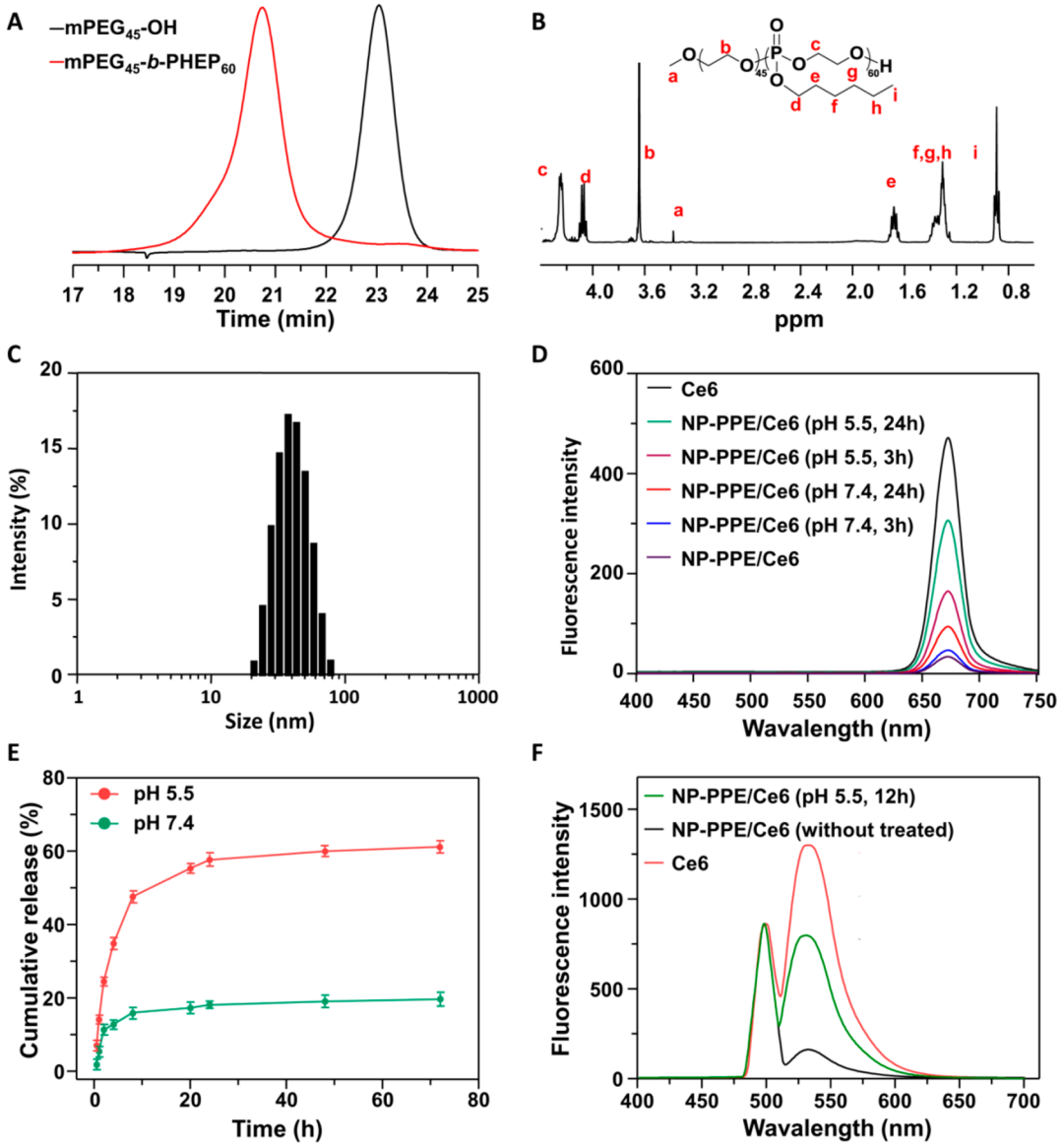

Figure 1. (A) GPC spectra of the macroinitiator $mPEG_{45}$-OH and diblock copolymer $mPEG_{45}$-*b*-$PHEP_{60}$. (B) ^1H NMR spectra of $mPEG_{45}$-*b*-$PHEP_{60}$ (in $CDCl_3$). (C) Size distribution of NP-PPE/Ce6 measured by DLS. (D) Fluorescence spectrum of NP-PPE/Ce6 with incubates in different conditions and (E) Ce6 release from the nanocarrier at pH 7.4 (green line) and pH 5.5 (red line) conditions. (F) Fluorescence spectrum of DCFH incubated with Ce6 and NP-PPE/Ce6 after NIR laser irradiation.

demonstrated that all the resonances could be assigned to the corresponding protons. The degrees of polymerization of copolymers were calculated by integrals of proton resonance of PEG backbone (b, 3.68 ppm) to methylene protons of PHEP backbone (c, 4.25 ppm). Thus, the obtained copolymer was denoted as $mPEG_{45}$-*b*-$PHEP_{60}$ (the subscript number represents degree of polymerization of each block).

By using the obtained amphiphilic mPEG-*b*-PHEP copolymer, the Ce6 encapsulated nanocarrier NP-PPE/Ce6 was prepared. The size and PDI of the NP-PPE/Ce6 was measured by DLS. The average size of NP-PPE/Ce6 was was 44.4 ± 4.3 nm (Figure 1C), and the PDI was about 0.108, indicating that the nanocarriers exhibited a narrow particle size distribution. The morphology of NP-PPE/Ce6 was observed by TEM (Figure S1), showing a compact and spherical morphology. In addition, the NP-PPE/Ce6 showed neutral surface charge with the zeta potential of −2.6 ± 1.3 mV.

A delivery system, which was capable of delivering drug to tumor cells, must keep stability before reaching the tumor tissue.[33] To monitor the stability of nanocarriers, NP-PPE/Ce6 was incubated in PBS containing 10% FBS at 37 °C. Then, the sizes change was monitored by DLS at different incubation time points. As shown in Figure S2, the size of NP-PPE/Ce6 particles did not show significantly changed, and the all the PDI values were less than 0.2, indicating that Ce6 encapsulated nanocarriers NP-PPE/Ce6 could keep stabilization in the blood environment.

One key point for drug delivery systems is keeping the drug encapsulated in nanocarrier before reaching the target cells but rapidly releasing once enter into the target cell.[34,35] To demonstrate the release behavior of NP-PPE/Ce6, its fluorescence, which was quenched after encapsulation, was first monitored in different conditions. The NP-PPE/Ce6 was incubated in PB buffer at pH 7.4 and 5.5 to mimic extracellular conditions and intracellular conditions. As shown in Figure 1D,

DOI: 10.1021/acsami.5b05724
ACS Appl. Mater. Interfaces 2015, 7, 18856−18865

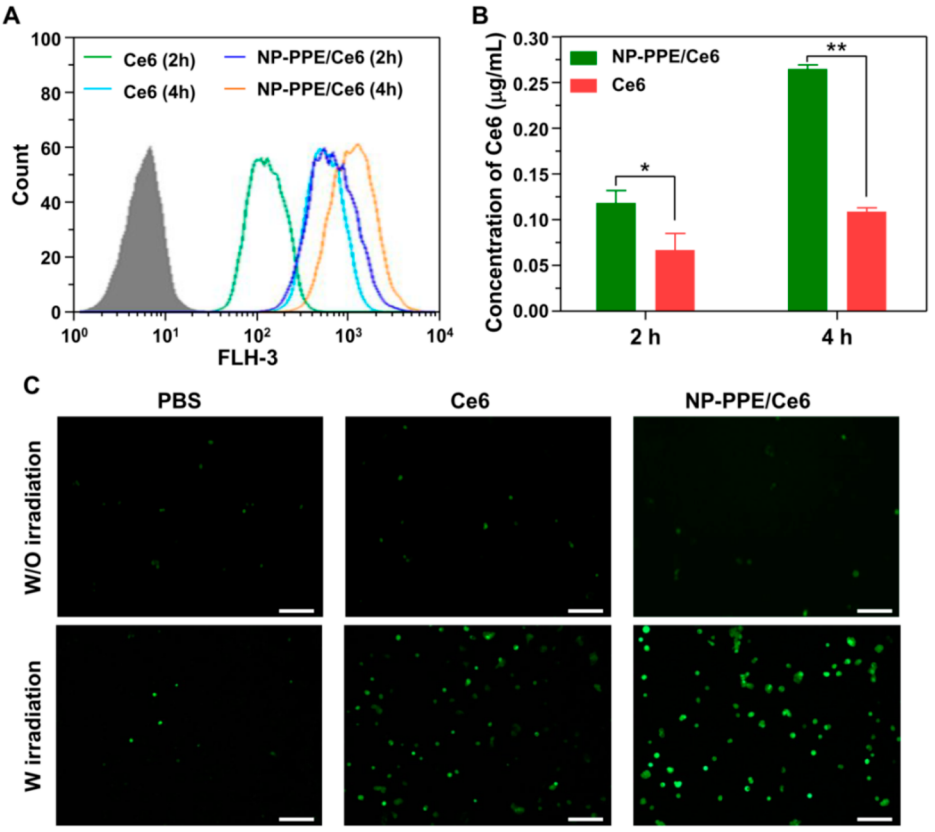

Figure 2. Cellular uptake of free Ce6 and NP-PPE/Ce6 (A) FACS curve and (B) quantitative Ce6 concentration in the BxPC-3 cancer cells. (C) CLSM image of cells incubated with DCFH-DA and then treated with free Ce6 and NP-PPE/Ce6 with NIR laser irradiation. Scale bar = 100 μm. * $p < 0.05$, ** $p < 0.01$.

it could be found the weak recover of fluorescence when incubated with pH 7.4 PB buffer for 3 h, and only about 20% fluorescence recovery of Ce6 was detected. In contrast, after incubation in pH 5.5 PB buffer for 3 and 24 h, about 35% and 65% of fluorescence was recovered, respectively. This result implied that the nanocarrier NP-PPE/Ce6 could keep the Ce6 in the hydrophobic core in the neutral condition during circulation, but rapidly release the encapsulated Ce6 in the acid endosome or lysosome after internalization into cancer cells. To verify this speculation, the release kinetics of Ce6 from the NP-PPE/Ce6 was quantitatively determined at pH 7.4 and pH 5.5. At pH 7.4, only 20% Ce6 released from NP-PPE/Ce6 in 72 h (Figure 1E). On the contrary, the Ce6 release was significantly accelerated at pH 5.5, reaching 60%. A similar released profile of the encapsulated drug was also observed previously.[28] To demonstrate the reason, the CMC of $mPEG_{45}$-*b*-$PHEP_{60}$ at pH 7.4 and pH 5.5 was detected. From the sigmoidal shape curve in Figure S3, the CMC values were calculated as 1.3×10^{-3} mg/mL at pH 7.4 and 3.2×10^{-3} mg/mL at pH 5.5, respectively. These data demonstrated that the hydrophobicity of polyphosphoester core was decreased at pH 5.5 when compared with that at pH 7.4, which could result in the enhanced release of the encapsulated Ce6 at pH 5.5.

After laser irradiation, the photosensitizers Ce6 was capable of generating ROS to kill tumor cells. To demonstrate it, the amount of generated ROS was evaluated using nonfluorescent 2′-7′-dichlorofluorescin (DCFH) as an indicator. The DCFH can react with ROS to generate 2′,7′-dichlorofluorescein (DCF) with fluorescence emission ranging mainly from 505 to 545 nm in wavelength.[36] After pretreatment at pH 5.5 for 12 h, the NP-PPE/Ce6 was mixed DCFH solution, which was resulted from the chemical hydrolysis of DCFH-DA at basic pH. Then, the mixture solutions were exposed to laser (660 nm, 0.5 mW/cm^2) for 30 min. The fluorescence intensity of DCF, which responded to the generation of ROS, was analyzed by fluorescence spectrophotometer. As shown in Figure 1F, only a weak fluorescence signal of DCF could be found when Ce6 was encapsulated in the hydrophobic core of the nanoparticle. However, after pretreatment at pH 5.5 for 12 h, the generated ROS by NP-PPE/Ce6 significantly enhanced, which may be due to the rapid release of Ce6 from the NP-PPE/Ce6 in the acid condition (Figure 1E). As a positive control, the Ce6 showed a strong ability to produce ROS when exposed to the NIR laser.

Cellular Uptake and Intracellular ROS Generation of NP-PPE/Ce6. As reported, the photosensitizer Ce6 was inefficiently internalized by cancer cells.[37,38] Compared with free Ce6, NP-PPE/Ce6 might be able to promote cellular internalization of the Ce6 by endocytosis pathway. To demonstrate it, the NP-PPE/Ce6 and free Ce6 were incubated with human pancreatic cancer cells BxPC-3 at a Ce6 concentration of 2.5 μg/mL. After incubation at 37 °C for 2 or 4 h, intracellular Ce6 fluorescence was detected by flow cytometry. As shown in Figure 2A, the cells incubated with NP-PPE/Ce6 exhibited much stronger intracellular Ce6 fluorescence signals than that incubated with free Ce6 at either 2 or 4 h, indicating that cellular uptake of the Ce6 was enhanced with the delivery of polymeric nanocarrier. Additionally, the cellular uptake was further quantitatively analyzed by determining the intracellular concentration of Ce6 HPLC. As shown in Figure 2B, the amount of intracellular Ce6 following incubation with NP-PPE/Ce6 was about 1.5-fold at 2 h and

DOI: 10.1021/acsami.5b05724
ACS Appl. Mater. Interfaces 2015, 7, 18856−18865

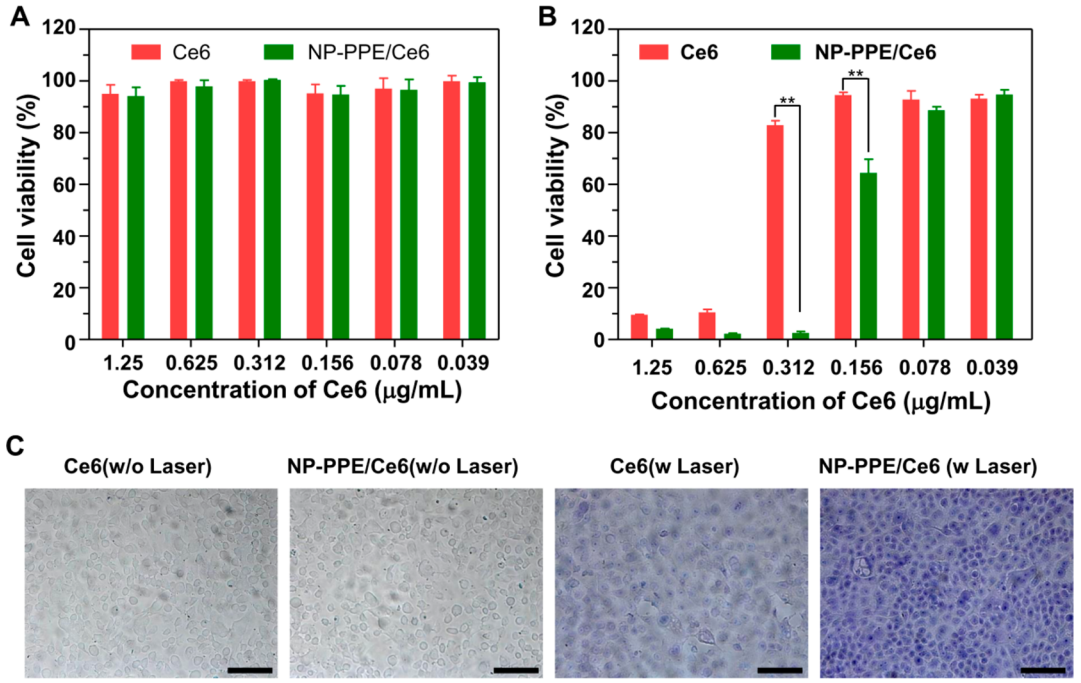

Figure 3. Photodynamic therapeutic efficacy in vitro. The cytotoxicity of NP-PPE/Ce6 and free Ce6 performance in BxPC-3 cells without (A) and with (B) NIR laser (660 nm) irradiation. (C) Image of apoptosis cells stained by trypan blue after treatment with different formulations. Scale bar = 50 μm. ** $p < 0.01$.

2-fold at 4 h greater than that treated with free Ce6. The results from HPLC and flow cytometry clearly demonstrated that NP-PPE/Ce6 could enhance the intracellular uptake of DOX in BxPC3 cells.

In addition, the intracellular distribution of Ce6 was observed by confocal laser scanning microscopy (CLSM). As shown in Figure S4, it could be clearly observed that the cells incubated with NP-PPE/Ce6 exhibited much stronger intracellular fluorescence signals in the cytoplasm compared to the cells treated with free Ce6. These results indicated that more photosensitizer Ce6 can be delivered into BxPC3 cells following incubation with NP-PPE/Ce6.

After internalization into BxPC3 cells, generation of cytotoxic ROS to kill the tumor cells is critical in photodynamic therapy. To monitor the generation of ROS after NIR irradiation, we used a reactive oxygen species assay kit DCFH-DA. The DCFH-DA can passively diffuse into cancer cells and transformed into nonfluorescent DCFH, which can easily react with ROS to generate DCF with fluorescence emission ranging mainly from 505 to 545 nm in wavelength. The amount of ROS produced by NP-PPE/Ce6 could be evaluated by the fluorescence intensity of DCF. As shown in Figure 2C, a slight green fluorescence was observed in the untreated control cells, indicating that only a few ROS were present inside the BxPC-3 cells. Meanwhile, either the NP-PPE/Ce6 or free Ce6 without laser irradiation exhibit almost similar fluorescence intensity as the PBS control group, implying that both group without laser irradiation could not product any additional ROS. In contrast, cells treated with either the NP-PPE/Ce6 or free Ce6 and then irradiated by 660 nm laser shown elevated intracellular green fluorescence, especially NP-PPE/Ce6 group exhibited strongest intracellular fluorescence in BxPC-3 cells after irradiation. These results demonstrated that the ROS could be selectively generated in BxPC-3 cells treated with NP-PPE/Ce6 or free Ce6 plus irradiation, and more ROS was generated after treatment with NP-PPE/Ce6, which may be because the polyphosphoester based nanocarriers can promote the cellular internalization of Ce6 and rapid intracellular release.

Photodynamic Therapeutic Efficacy in Vitro. The enhanced generation of ROS in BxPC-3 cells by incubation with NP-PPE/Ce6 may be accompanied by an improved PDT efficacy to kill the cancer cells. To demonstrate this, MTT viability assay were carried out for BxPC-3 cells after various treatments. As expected, both free Ce6 and NP-PPE/Ce6 showed negligible cytotoxicity without irradiation (Figure 3A). After exposing to laser (660 nm, 0.5 mW/cm^2) for 20 min, the cell viability decreased in a dose-dependent manner for free Ce6 and NP-PPE/Ce6. In addition, NP-PPE/Ce6 was more effectively reduced cell viability than the free Ce6. For example, for BxPC-3 cells treated with NP-PPE/Ce6 at a Ce6 dose of 0.312 μg/mL, the viability was lower than 5% after irradiation, while more than 80% of BxPC-3 cells survived at the same dose for free Ce6 (Figure 3B). Additionally, the apoptosis cells were further analyzed by trypan blue staining. In accordance with the result of MTT assay, after incubation with these formulations and subsequent NIR irradiation, a large number of apoptotic cells dyed blue were observed for NP-PPE/Ce6 group, while fewer apoptotic cells were detected in the free Ce6 group. In addition, the NP-PPE/Ce6 and free Ce6 without laser irradiation did not show apoptosis when compared with the PBS group. These results demonstrated that treatment with NP-PPE/Ce6 plus NIR irradiation exhibited excellent killing ability compared to that of free Ce6, which was consistent with the improved Ce6 internalization and enhanced generation of ROS within tumor cells (Figure 3C).

Pharmacokinetics and Biodistribution of Ce6 and NP-PPE/Ce6 in Vivo. It has been demonstrated that free Ce6 is rapidly cleared from the blood, resulting in insufficient accumulation in tumor tissue.[39] As reported, PEG stabilized nanocarriers were capable of simultaneously extending circulation

DOI: 10.1021/acsami.5b05724
ACS Appl. Mater. Interfaces 2015, 7, 18856−18865

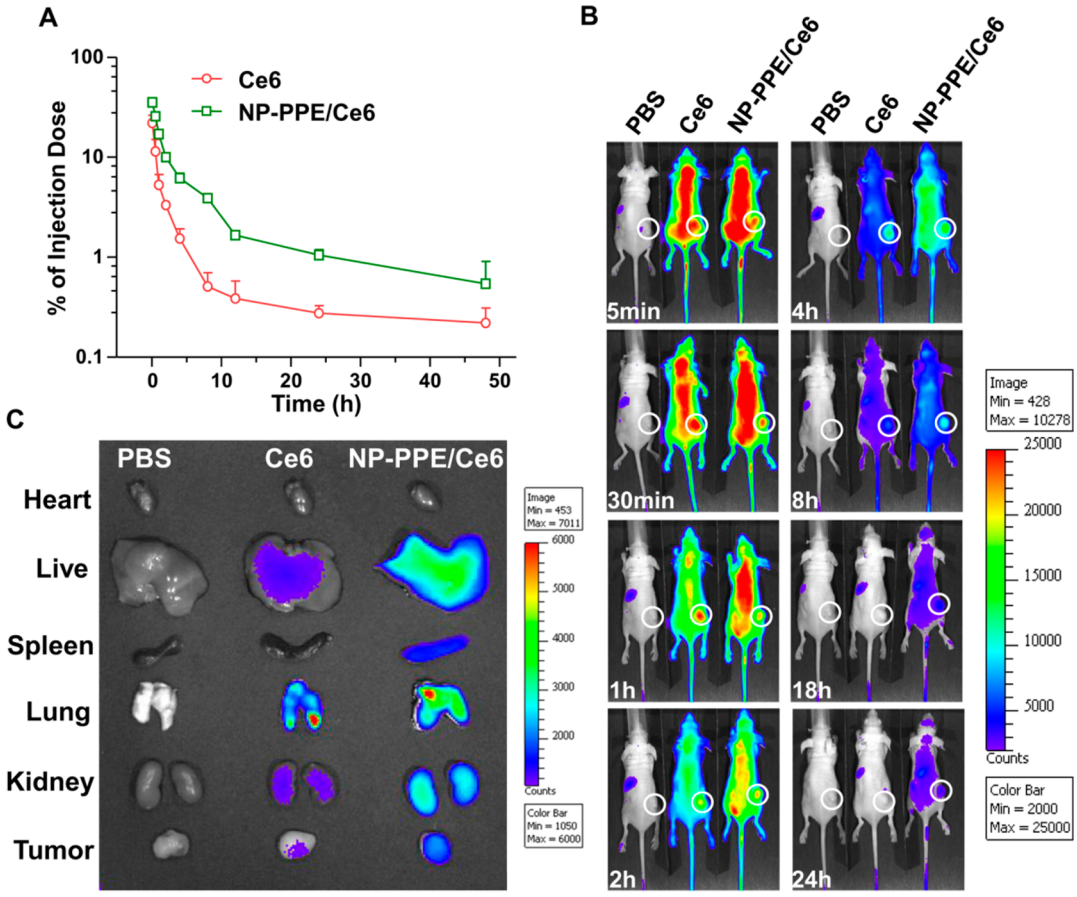

Figure 4. Pharmacokinetics and biodistribution of free Ce6 and NP-PPE/Ce6 in vivo. (A) Pharmacokinetics studies of the various formulations. The formulations were intravenously injected into ICR mice at an equivalent Ce6 dose of 2.5 mg/kg per mouse. Data are presented as mean ± SD (n = 3). (B) Fluorescence images of BxPC-3 xenograft-bearing mice after intravenous (i.v.) injection of PBS (left), Ce6 (middle), and NP-PPE/Ce6 (right) at different times. The tumor sites were denoted by white circular. (C) Ex vivo images of organs such as heart, liver, spleen, lung, kidney, and tumors excised at 24 h postinjection of PBS, free Ce6, and NP-PPE/Ce6.

time in blood and enhancing drug accumulation in tumors. To demonstrate it, both NP-PPE/Ce6 and free Ce6 were intravenously injected into ICR mice. At the predetermined time, the blood was collected, and the plasma level of Ce6 was determined by HPLC. As shown in Figure 4A, NP-PPE/Ce6 exhibited prolonged circulation time ($T_{1/2}$> 10 h) in the bloodstream compared to free Ce6. Meanwhile, the NP-PPE/Ce6 significantly increased the area under the curve (AUC) in blood in contrast to the free Ce6. The mean residence time (MRT) of NP-PPE/Ce6 was 5-fold higher than that of free Ce6 (Table S1).

Following intravenous injection of NP-PPE/Ce6 or free Ce6 into nude mice bearing BxPC-3 xenografts, the biodistributions of NP-PPE/Ce6 and free Ce6 was determined by Xenogen IVIS Lumina system. As shown in Figure 4B, almost all of the Ce6 had been cleared in 18 h, while the NP-PPE/Ce6 group showed remarkable extended retention in blood circulation, indicating that the retention time of NP-PPE/Ce6 was much longer than free Ce6. In addition, the Ce6 fluorescence intensity from NP-PPE/Ce6 in the tumor site was significantly higher than that from free Ce6 at all-time points. In addition, the organs of interest were collected for fluorescence imaging after 24 h postinjection. As shown in Figure 4C, the mice injected with NP-PPE/Ce6 exhibited significantly enhanced accumulation of Ce6 in tumor in comparison with those injected with free Ce6. In addition, fluorescence signals of Ce6 were clearly detected in kidney and liver, which also been indicated in Figure S5 that the tumor-to-kidney and tumor-to-liver ratio was low, implying that the NP-PPE/Ce6 was gradually cleared by these organs.

Photodynamic Therapeutic Antitumor Activity in BxPC-3 Tumor-Bearing Mice. According to the results of the enhanced accumulation in tumor tissue, we speculated that treatment with NP-PPE/Ce6 should show an enhanced antitumor efficacy for BxPC-3 tumor by photodynamic therapy. To demonstrate it, BxPC-3 tumor-bearing mice were randomly divided into different groups and treated with PBS, free Ce6 and NP-PPE/Ce6. After 4 h postinjection, the tumor was irradiated with NIR light (660 nm, 0.5 W/cm^2) for 30 min. Mice intravenously injected NP-PPE/Ce6 but without laser irradiation were also used as the control. As shown in Figures 5A and S6, the tumor growth was significantly inhibited after treatment with NP-PPE/Ce6 plus irradiation (NP-PPE/Ce6 (without laser)), the volume of the tumor even reduced about 60% compare to the original size. However, treatment with free Ce6 plus NIR (Ce6 (with laser)) laser irradiation resulted in slight inhibition of tumor growth. In addition, administration of NP-PPE/Ce6 without NIR irradiation (NP-PPE/Ce6 (without laser)) did not inhibit BxPC-3 tumor growth in comparison to PBS, indicating that the photosensitizer Ce6 did not exhibit phototoxicity without laser stimulation. In addition, the tumor was excised after the last measurement, and the weight of the

DOI: 10.1021/acsami.5b05724
ACS Appl. Mater. Interfaces 2015, 7, 18856−18865

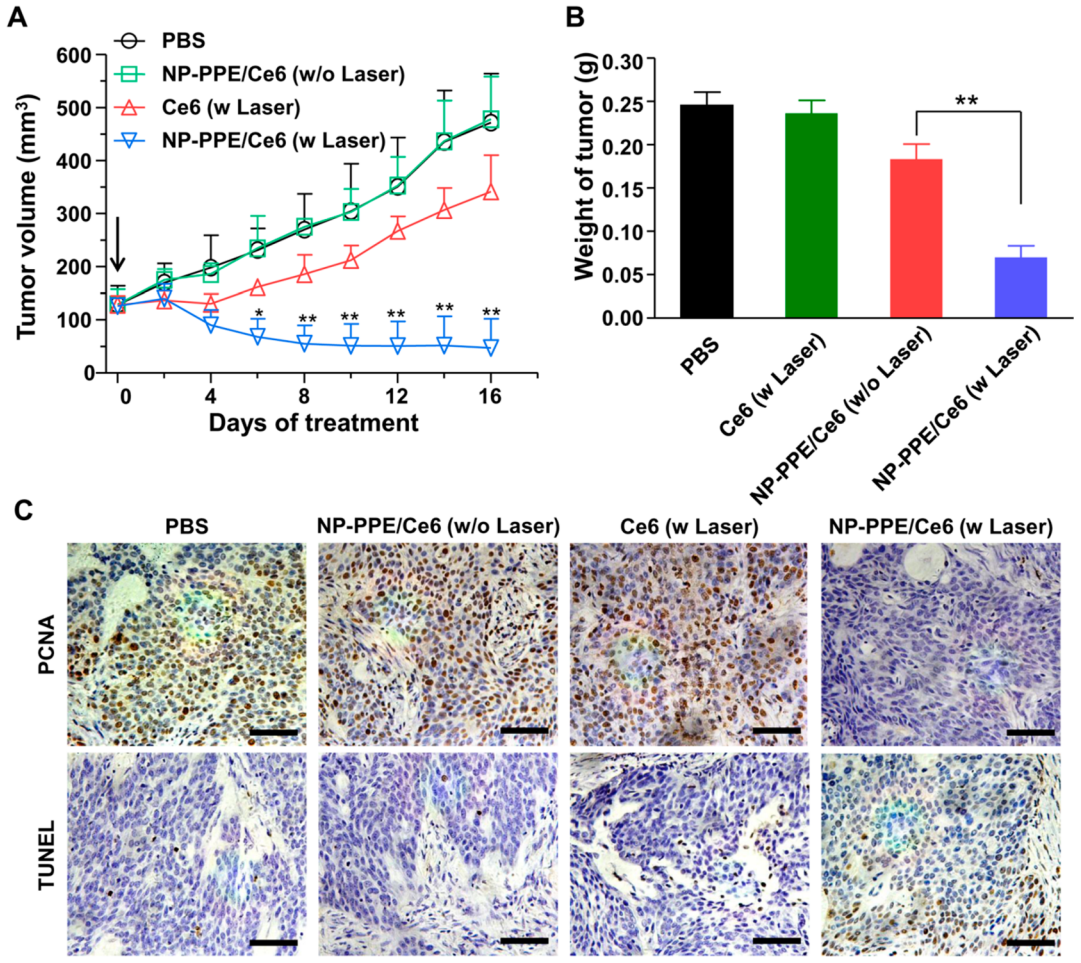

Figure 5. In vivo antitumor activity in human xenograft pancreatic tumor model after photodynamic therapy. (A) Inhibition of tumor growth in BxPC-3 human pancreatic cancer model after treatment with different formulations. Mice were intravenously administered an equivalent Ce6 dose of 2.5 mg per kg mouse body weight on days 0. Data are presented as mean ± SD (n = 5). * p < 0.05, ** p < 0.01. (B) Weight of the BxPC-3 tumor mass excised after the last measurement. Data are presented as mean ± SD (n = 5). (C) PCNA and TUNEL analyses of tumor tissues after treatment with various formulations. PCNA-positive proliferating cells are stained brown, TUNEL-positive apoptotic cells are stained brown. Scale bar =50 μm.

tumor mass was assessed (Figure 5B). The mean tumor weight treated with NP-PPE/Ce6 without laser irradiation or with free Ce6 plus laser irradiation was 3-fold and 2-fold of that treated with NP-PPE/Ce6 plus laser irradiation. In addition, none of the treatment formulations caused obvious body weight loss during the course of the study (Figure S7), and the histological analyses by hematoxylin and eosin (H&E) of the organs after treatment did not show obvious biology toxicity (Figure S8), eliminating safety concerns about the systems. Moreover, cell proliferation and apoptosis in tumor tissue were also analyzed by immunohistochemical (Figure 5C). Administration of NP-PPE/Ce6 plus NIR irradiation markedly enhanced efficiency of treatment in inhibiting proliferation and inducing apoptosis in BxPC-3 tumor cells. Overall, these results demonstrated that polyphosphoester based polymeric nancarriers as the delivery system of photosensitizer Ce6 has great potentials for PDT of tumors.

CONCLUSIONS

In this work, we successfully developed polyphosphoester-based nanocarrier to deliver the photosensitizer Ce6 to the cancer cell. We encapsulated the photosensitizer Ce6 into mPEG-*b*-PHEP nanocarriers. The obtained polyphosphoester-based nanocarrier NP-PPE/Ce6 exhibited a diameter of 40 nm and neutral surface charge. With the delivery by NP-PPE/Ce6, the blood circulation time of photosensitizer Ce6 significantly was prolonged, and the accumulation of Ce6 in tumor was enhanced. After internalization, the encapsulated Ce6 was rapidly released from the NP-PPE/Ce6, resulting in the improved generation of ROS compared to that of free Ce6. Therefore, administration of NP-PPE/Ce6 plus NIR irradiation markedly enhanced the inhibiting of BxPC-3 tumor growth, indicating the great potentials of polyphosphoester-based nanocarrier as the delivery system of photosensitizer for PDT of pancreatic cancer.

ASSOCIATED CONTENT

Supporting Information

The Supporting Information is available free of charge on the ACS Publications website at DOI: 10.1021/acsami.5b05724.

Fluorescent spectrum of Ce6-loaded micelles, body weights of mice (PDF)

AUTHOR INFORMATION

Corresponding Authors

*E-mail: yuyuemd@163.com (Y.Y.).
*E-mail: yangxz@hfut.edu.cn (X.-Z.Y.).

DOI: 10.1021/acsami.5b05724
ACS Appl. Mater. Interfaces 2015, 7, 18856−18865

Author Contributions

[§]F.D., H.-J.L., and J.-X.W. contributed equally to this work.

Notes

The authors declare no competing financial interest.

■ ACKNOWLEDGMENTS

This work was supported by the Ministry of Science and Technology of the People's Republic of China (2014AA020708), the National Natural Science Foundation of China (51473043, 51203145, 21304028), and the Fundamental Research Funds for the Central Universities (2014HGCH0014). The authors would also like to acknowledge Prof. Jun Wang (University of Science & Technology of China) for support.

■ REFERENCES

(1) Hidalgo, M. Pancreatic Cancer. *N. Engl. J. Med.* **2010**, *362*, 1605−1617.
(2) Edwards, B. K.; Noone, A. M.; Mariotto, A. B.; Simard, E. P.; Boscoe, F. P.; Henley, S. J.; Jemal, A.; Cho, H.; Anderson, R. N.; Kohler, B. A.; Eheman, C. R.; Ward, E. M. Annual Report to the Nation on the Status of Cancer, 1975−2010, Featuring Prevalence of Comorbidity and Impact on Survival Among Persons with Lung, Colorectal, Breast, or Prostate Cancer. *Cancer* **2014**, *120*, 1290−1314.
(3) Wang, Y. Z.; Fan, W.; Dai, X.; Katragadda, U.; Mckinley, D.; Teng, Q.; Tan, C. Enhanced Tumor Delivery of Gemcitabine via PEG-DSPE/TPGS Mixed Micelles. *Mol. Pharmaceutics* **2014**, *11*, 1140−1150.
(4) Chung, W. G.; Sandoval, M. A.; Sloat, B. R.; Lansakara, D. S. P.; Cui, Z. R. Stearoyl Gemcitabine Nanoparticles Overcome Resistance Related to the Over-Expression of Ribonucleotide Reductase Subunit M1. *J. Controlled Release* **2012**, *157*, 132−140.
(5) Zmijewska-Tomczak, M.; Milecki, P.; Olek-Hrab, K.; Hojan, K.; Golusinski, W.; Rucinska, A.; Adamska, A. Factors Influencing Quality of Life in Patients During Radlotherapy for Head and Neck Cancer. *Arch. Med. Sci.* **2014**, *6*, 1153−1159.
(6) Idris, N. M.; Gnanasammandhan, M. K.; Zhang, J.; Ho, P. C.; Mahendran, R.; Zhang, Y. In vivo Photodynamic Therapy Using Upconversion Nanoparticles as Remote-Controlled Nanotransducers. *Nat. Med.* **2012**, *18*, 1580−U190.
(7) Chen, H. B.; Xiao, L.; Anraku, Y.; Mi, P.; Liu, X. Y.; Cabral, H.; Inoue, A.; Nomoto, T.; Kishimura, A.; Nishiyama, N.; Kataoka, K. Polyion Complex Vesicles for Photoinduced Intracellular Delivery of Amphiphilic Photosensitizer. *J. Am. Chem. Soc.* **2014**, *136*, 157−163.
(8) Wang, X.; Liu, K.; Yang, G. B.; Cheng, L.; He, L.; Liu, Y. M.; Li, Y. G.; Guo, L.; Liu, Z. Near-Infrared Light Triggered Photodynamic Therapy in Combination with Gene Therapy Using Upconversion Nanoparticles for Effective Cancer Cell Killing. *Nanoscale* **2014**, *6*, 9198−9205.
(9) Yuan, Y.; Liu, J.; Liu, B. Conjugated-Polyelectrolyte-Based Polyprodrug: Targeted and Image-Guided Photodynamic and Chemotherapy with On-Demand Drug Release upon Irradiation with a Single Light Source. *Angew. Chem., Int. Ed.* **2014**, *53*, 7163−7168.
(10) Castano, A. P.; Demidova, T. N.; Hamblin, M. R. Mechanisms in Photodynamic Therapy: Part One-Photosensitizers, Photochemistry and Cellular Localization. *Photodiagn. Photodyn. Ther.* **2004**, *1*, 279−293.
(11) Oleinick, N. L.; Morris, R. L.; Belichenko, T. The Role of Apoptosis in Response to Photodynamic Therapy: What, Where, Why, and How. *Photochem. Photobiol. Sci.* **2002**, *1*, 1−21.
(12) Jang, Y. H.; Koo, G. B.; Kim, J. Y.; Kim, Y. S.; Kim, Y. C. Prolonged Activation of ERK Contributes to the Photorejuvenation Effect in Photodynamic Therapy in Human Dermal Fibroblasts. *J. Invest. Dermatol.* **2013**, *133*, 2265−2275.
(13) Krammer, B. Vascular Effects of Photodynamic Therapy. *Anticancer Res.* **2001**, *21*, 4271−4277.
(14) Master, A.; Livingston, M.; Sen Gupta, A. Photodynamic Nanomedicine in the Treatment of Solid Tumors: Perspectives and Challenges. *J. Controlled Release* **2013**, *168*, 88−102.
(15) Castano, A. P.; Mroz, P.; Hamblin, M. R. Photodynamic Therapy and Anti-Tumour Immunity. *Nat. Rev. Cancer* **2006**, *6*, 535−545.
(16) Master, A.; Livingston, M.; Sen Gupta, A. Photodynamic Nanomedicine in the Treatment of Solid Tumors: Perspectives and Challenges. *J. Controlled Release* **2013**, *168*, 88−102.
(17) Huang, Z. A Review of Progress in Clinical Photodynamic Therapy. *Technol. Cancer Res. Treat.* **2005**, *4*, 283−293.
(18) Liang, X. L.; Li, X. D.; Jing, L. J.; Yue, X. L.; Dai, Z. F. Theranostic Porphyrin Dyad Nanoparticles for Magnetic Resonance Imaging Guided Photodynamic Therapy. *Biomaterials* **2014**, *35*, 6379−6388.
(19) Park, Y.; Kim, H. M.; Kim, J. H.; Moon, K. C.; Yoo, B.; Lee, K. T.; Lee, N.; Choi, Y.; Park, W.; Ling, D.; Na, K.; Moon, W. K.; Choi, S. H.; Park, H. S.; Yoon, S. Y.; Suh, Y. D.; Lee, S. H.; Hyeon, T. Theranostic Probe Based on Lanthanide-Doped Nanoparticles for Simultaneous In Vivo Dual-Modal Imaging and Photodynamic Therapy. *Adv. Mater.* **2012**, *24*, 5755−5761.
(20) Tian, B.; Wang, C.; Zhang, S.; Feng, L. Z.; Liu, Z. Photothermally Enhanced Photodynamic Therapy Delivered by Nano-Graphene Oxide. *ACS Nano* **2011**, *5*, 7000−7009.
(21) Murakami, T.; Nakatsuji, H.; Inada, M.; Matoba, Y.; Umeyama, T.; Tsujimoto, M.; Isoda, S.; Hashida, M.; Imahori, H. Photodynamic and Photothermal Effects of Semiconducting and Metallic-Enriched Single-Walled Carbon Nanotubes. *J. Am. Chem. Soc.* **2012**, *134*, 17862−17865.
(22) Zhang, D.; Wu, M.; Zeng, Y. Y.; Wu, L. J.; Wang, Q. T.; Han, X.; Liu, X. L.; Liu, J. F. Chlorin e6 Conjugated Poly(dopamine) Nanospheres as PDT/PTT Dual-Modal Therapeutic Agents for Enhanced Cancer Therapy. *ACS Appl. Mater. Interfaces* **2015**, *7*, 8176−8187.
(23) Lucky, S. S.; Soo, K. C.; Zhang, Y. Nanoparticles in Photodynamic Therapy. *Chem. Rev.* **2015**, *115*, 1990−2042.
(24) Shan, J. N.; Budijono, S. J.; Hu, G. H.; Yao, N.; Kang, Y. B.; Ju, Y. G.; Prud'homme, R. K. Pegylated Composite Nanoparticles Containing Upconverting Phosphors and meso-Tetraphenyl porphine (TPP) for Photodynamic Therapy. *Adv. Funct. Mater.* **2011**, *21*, 2488−2495.
(25) Master, A. M.; Qi, Y. Z.; Oleinick, N. L.; Sen Gupta, A. EGFR-Mediated Intracellular Delivery of Pc 4 Nanoformulation for Targeted Photodynamic Therapy of Cancer: in vitro Studies. *Nanomedicine* **2012**, *8*, 655−664.
(26) Ling, D.; Bae, B. C.; Park, W.; Na, K. Photodynamic Efficacy of Photosensitizers under an Attenuated Light Dose via Lipid Nano-Carrier-Mediated Nuclear Targeting. *Biomaterials* **2012**, *33*, 5478−5486.
(27) Park, H.; Na, K. Conjugation of the Photosensitizer Chlorin e6 to Pluronic F127 for Enhanced Cellular Internalization for Photodynamic Therapy. *Biomaterials* **2013**, *34*, 6992−7000.
(28) Sun, C. Y.; Ma, Y. C.; Cao, Z. Y.; Li, D. D.; Fan, F.; Wang, J. X.; Tao, W.; Yang, X. Z. Effect of Hydrophobicity of Core on the Anticancer Efficiency of Micelles as Drug Delivery Carriers. *ACS Appl. Mater. Interfaces* **2014**, *6*, 22709−22718.
(29) Li, P. P.; Zhou, G. Y.; Zhu, X. Y.; Li, G. L.; Yan, P.; Shen, L. Y.; Xu, Q.; Hamblin, M. R. Photodynamic Therapy with Hyperbranched Poly(ether-ester) Chlorin(e6) Nanoparticles on Human Tongue Carcinoma CAL-27 Cells. *Photodiagn. Photodyn. Ther.* **2012**, *9*, 76−82.
(30) Lin, J.; Wang, S. J.; Huang, P.; Wang, Z.; Chen, S. H.; Niu, G.; Li, W. W.; He, J.; Cui, D. X.; Lu, G. M.; Chen, X. Y.; Nie, Z. H. Photosensitizer-Loaded Gold Vesicles with Strong Plasmonic Coupling Effect for Imaging-Guided Photothermal/Photodynamic Therapy. *ACS Nano* **2013**, *7*, 5320−5329.
(31) Yuan, Y. Y.; Liu, B. Self-Assembled Nanoparticles Based on PEGylated Conjugated Polyelectrolyte and Drug Molecules for Image-Guided Drug Delivery and Photodynamic Therapy. *ACS Appl. Mater. Interfaces* **2014**, *6*, 14903−14910.

DOI: 10.1021/acsami.5b05724
ACS Appl. Mater. Interfaces 2015, 7, 18856−18865

(32) Liu, P.; Yue, C. X.; Sheng, Z. H.; Gao, G. H.; Li, M. X.; Yi, H. Q.; Zheng, C. F.; Wang, B.; Cai, L. T. Photosensitizer-Conjugated Redox-Responsive Dextran Theranostic Nanoparticles for Near-Infrared Cancer Imaging and Photodynamic Therapy. *Polym. Chem.* **2014**, *5*, 874−881.
(33) Sun, C. Y.; Dou, S.; Du, J. Z.; Yang, X. Z.; Li, Y. P.; Wang, J. Doxorubicin Conjugate of Poly(Ethylene Glycol)-Block Polyphosphoester for Cancer Therapy. *Adv. Healthcare Mater.* **2014**, *3*, 261−272.
(34) Li, H. J.; Wang, H. X.; Sun, C. Y.; Du, J. Z.; Wang, J. Shell-Detachable Nanoparticles Based on a Light-Responsive Amphiphile for Enhanced siRNA Delivery. *RSC Adv.* **2014**, *4*, 1961−1964.
(35) Zou, J.; Zhang, F. W.; Zhang, S. Y.; Pollack, S. F.; Elsabahy, M.; Fan, J. W.; Wooley, K. L. Poly(ethylene oxide)-block-Polyphosphoester-graft-Paclitaxel Conjugates with Acid-Labile Linkages as a pH-Sensitive and Functional Nanoscopic Platform for Paclitaxel Delivery. *Adv. Healthcare Mater.* **2014**, *3*, 441−448.
(36) Rovira-Llopis, S.; Rocha, M.; Falcon, R.; de Pablo, C.; Alvarez, A.; Jover, A.; Hernandez-Mijares, A.; Victor, V. M. Is Myeloperoxidase a Key Component in the ROS-Induced Vascular Damage Related to Nephropathy in Type 2 Diabetes? *Antioxid. Redox Signaling* **2013**, *19*, 1452−1458.
(37) Zhang, H.; Peng, C.; Yang, J. Z.; Lv, M.; Liu, R.; He, D. N.; Fan, C. H.; Huang, Q. Uniform Ultrasmall Graphene Oxide Nanosheets with Low Cytotoxicity and High Cellular Uptake. *ACS Appl. Mater. Interfaces* **2013**, *5*, 1761−1767.
(38) Tu, C. L.; Zhu, L. J.; Li, P. P.; Chen, Y.; Su, Y.; Yan, D. Y.; Zhu, X. Y.; Zhou, G. Y. Supramolecular Polymeric Micelles by the Host-Guest Interaction of Star-Like Calix[4]arene and Chlorin e6 for Photodynamic Therapy. *Chem. Commun.* **2011**, *47*, 6063−6065.
(39) Lim, S. B.; Banerjee, A.; Onyuksel, H. Improvement of Drug Safety by the Use of Lipid-Based Nanocarriers. *J. Controlled Release* **2012**, *163*, 34−45.

DOI: 10.1021/acsami.5b05724
ACS Appl. Mater. Interfaces 2015, 7, 18856−18865